

Low-energy electron microscopy and spectroscopy with ESCHER: Status and prospects

S. M. Schramm
J. Kautz
A. Berghaus
O. Schaff
R. M. Tromp
S. J. van der Molen

We describe the layout and the capabilities of a new aberration-corrected low-energy electron microscopy (LEEM) and photoemission electron microscopy (PEEM) facility, which features real- and reciprocal-space spectroscopy. This new setup, named Electronic, Structural, and Chemical Nanoimaging in Real Time (ESCHER), was recently installed at Leiden University. It has three major instrumentation-related goals. First, we aim to reach the ultimate spatial resolution facilitated by aberration correction using an electron mirror, together with advanced electron detection. Second, we want to develop and exploit the spectroscopic possibilities of LEEM and PEEM in a standard laboratory environment. To this end, ESCHER is equipped with an inline energy filter and advanced photon sources. Third, we plan to extend the sample temperature range down to approximately 10 K, which is significantly lower than that achieved to date. Combined, these efforts will broaden the scientific reach of LEEM and PEEM beyond the areas of surface and materials science and into the realms of biosciences and life sciences. Here, we also present images of the first experiments performed with ESCHER focused on the growth of graphene on SiC(0001).

Introduction

Low-energy electron microscopy (LEEM) and photoemission electron microscopy (PEEM) are powerful surface-science techniques. They enable real-time *in situ* imaging of surfaces and interfaces at elevated temperatures and with nanometer resolution [1–4]. In this contribution, we describe an advanced aberration-corrected LEEM/PEEM facility, i.e., Electronic, Structural, and Chemical Nanoimaging in Real Time (ESCHER), which was recently installed at Leiden Center for Ultramicroscopy, Leiden University. The scientific goals of this Dutch national facility are threefold: 1) to reach the ultimate spatial resolution promised by electron-mirror-based aberration correction; 2) to develop, optimize, and exploit the spectroscopic possibilities afforded by inline, real-space, and reciprocal-space resolved electron energy spectroscopy;

and 3) to extend the sample temperature range to cryogenic temperatures in the 10-K range or lower. In combination, these three goals will facilitate novel interdisciplinary experiments in scientific areas such as nanoelectronics, condensed matter physics, and biophysics. This will significantly broaden the scientific impact of LEEM/PEEM beyond the traditional areas of surface and materials science.

In this paper, we give a comprehensive description of the ESCHER facility and its current capabilities. We also present the first experimental results obtained during the installation and testing phase of the ESCHER instrument. Next, we discuss the theoretical limit resolution for the aberration-corrected LEEM and PEEM and the additional steps necessary to reach this ultimate resolution with our instrument. Finally, we discuss the design concept of a cryogenic sample stage and an objective lens system, which is capable of reaching sample temperatures of 10 K or below in an ultrahigh-vacuum environment. The challenge is to achieve this without sacrificing sample exchange and

Digital Object Identifier: 10.1147/JRD.2011.2150691

© Copyright 2011 by International Business Machines Corporation. Copying in printed form for private use is permitted without payment of royalty provided that (1) each reproduction is done without alteration and (2) the Journal reference and IBM copyright notice are included on the first page. The title and abstract, but no other portions, of this paper may be copied by any means or distributed royalty free without further permission by computer-based and other information-service systems. Permission to republish any other portion of this paper must be obtained from the Editor.

0018-8646/11/\$5.00 © 2011 IBM

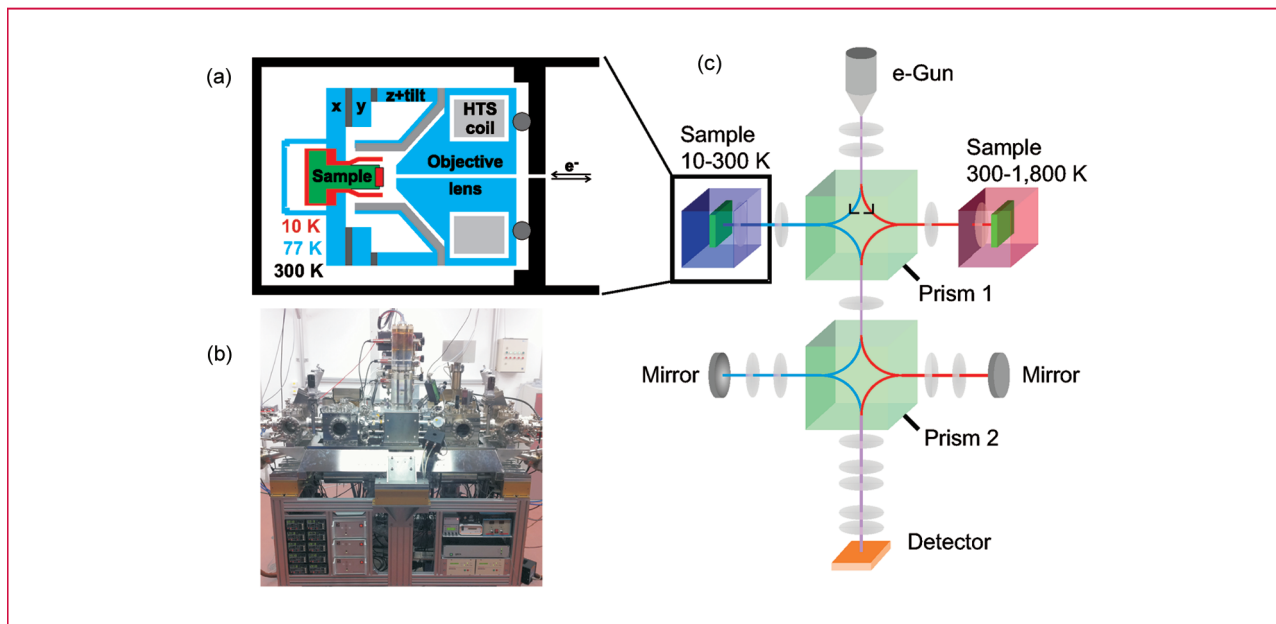


Figure 1

ESCHER setup: (a) Schematic of the low-temperature sample chamber design concept; (b) photograph of the ESCHER setup; (c) schematic diagram of the ESCHER setup. The sample chamber for experiments at elevated temperatures (300–1,800 K) is located on the right-hand side of the central gun/projector column. The cryogenic sample chamber (10–300 K) is placed on the left-hand side of the central column. The respective electron paths are indicated by the purple and blue (cryogenic temperature) and the purple and red (high temperature) lines. (HTS: high-temperature superconductor.)

positioning capabilities, electron spectroscopic capabilities, or aberration correction.

ESCHER setup

The ESCHER setup is based on the commercially available FE-LEEM P90 instrument (SPECS GmbH, Berlin) designed by IBM [5]. **Figure 1(a)** shows a schematic diagram of the low-temperature sample chamber design concept. **Figure 1(b)** shows a photograph of the ESCHER setup. In the center, we see the vertical electron column that extends from the gun (top) to the image screen (bottom). Extending to the sides are the high- (right) and low-temperature (left) imaging chambers, plus their respective sample loadlock systems. In a high-temperature LEEM experiment, the electrons follow the optical axis indicated in purple and red in **Figure 1(c)**. The cold field-emission gun generates an electron beam with an energy of 15 keV. A combination of a gun lens and a condenser lens serves to focus the electron beam with variable magnification. Next, a magnetic prism array, with electron optical properties that closely resemble those of a thin lens, deflects the electrons by 90° toward the objective lens and the sample. The sample itself is held at a negative potential close to that of the field emitter in the electron gun. Hence, the electrons can be decelerated to an energy in the range of 0–100 eV. After interaction with the sample, the electrons are

reflected back into the vacuum and again accelerated to 15 keV in the direction of the magnetic prism array. The objective lens, plus a transfer lens, places a magnified image of the sample on the diagonal plane of the prism array. The prism array deflects the electrons again by 90° toward a second prism array. The midplane between these two prism arrays coincides with a diffraction plane. In a LEEM experiment, this is where the low-energy electron diffraction pattern is located. In a PEEM experiment, this is where one finds the angular distribution of the photoelectrons. An electrostatic lens located in this same plane transfers the image rotation-free from the diagonal of the first magnetic prism array to the diagonal plane of the second prism array. The latter deflects the electrons once more by 90° toward a four-element electron mirror. The purpose of this electron mirror is to compensate both the chromatic and spherical aberrations of the objective lens. This improves the image resolution from approximately 5 to less than 1 nm, as predicted by full wave-optical resolution calculations (see section below). At the same time, the transmission of the instrument is increased by about a factor of 10 (see below). On the path toward the mirror, an uncorrected image is placed in the mirror object plane. The mirror reflects the image into that same plane, with a magnification of 1, removing chromatic and spherical aberration in the reflection process. The electrons then return to the second prism array,

with the corrected image again located on the prism diagonal. After this final deflection of 90° , the electrons enter the projector system. By changing the settings of the projector column, either the real space image or the diffraction pattern can be projected onto the image screen.

In PEEM experiments, the emitted electrons are accelerated away from the sample and follow the same path as in a LEEM experiment. To generate photoelectrons, we can illuminate the sample using either a Hg discharge lamp or a focused He I/He II discharge source.

The base pressure in the ESCHER setup is about 10^{-10} mbar. Experiments can be performed at pressures up to approximately 10^{-5} mbar. Samples are cleaned *in situ*, either by heating via electron bombardment or by sputtering, using a differentially pumped scanning small spot ion source. Because images are obtained in real time, processes such as growth, interface formation, phase transitions, and phase transformations can be followed at high resolution and at video rate. The high-temperature imaging chamber is equipped with evaporator sources, as well as with chemical vapor deposition facilities with a direct line of sight to the sample. A Hiden Hal 7 quadrupole mass spectrometer with a mass range of 500 u gives tight control over these processes.

One of the unique features of ESCHER is the implementation of two sample chambers positioned around a single vertical gun/projector column. This provides two experimental locations using only one set of central column components. In the right chamber, the sample temperature can be varied between 300 and 1,800 K. The left chamber will be equipped with a cryogenic stage and an objective lens to cool the sample to around 10 K (see section below). By changing the polarity of the magnetic field in the prisms, we will be able to switch between the high- and low-temperature imaging systems [see Figure 1(c)]. Note that ESCHER is equipped with two aberration-correcting mirrors. For the aberration correction to work, the 90° deflection angles provided by the magnetic prism arrays must always be of the same sense (either clockwise or counterclockwise) to maintain the proper symmetries in the imaging optics.

For distinguishing nanostructures, the highest possible spatial resolution, as well as the highest possible electron transmission, is desired. Clearly, electronic and mechanical stabilities are a first requirement for this. We minimize the effects of chromatic aberrations by using a cold field emitter with a small energy spread (0.25 eV). Even with the correction of the chromatic aberration coefficient C_c , higher rank aberrations make the choice of the electron source relevant. This is particularly important for experiments at electron energies at the sample below 5 eV, as preferred for imaging organic systems. Passive electromagnetic shielding of the entire electron path and active vibration isolation reduce external influences to a minimum.

To extend the possibilities even further, the ESCHER setup has been equipped with an inline energy filter [6].

This filter is based on the fact that the deflection angle of a magnetic prism is highly sensitive to the precise energy of the electrons. The current design provides an energy resolution of 150–200 meV at 15-keV electron energy ($\Delta E/E \sim 1.10^{-5}$), without the need for deceleration optics. In this configuration, the microscope can be used as a space- and angle-resolved ultraviolet photoemission spectroscopy facility for surface electronic structure studies. By combining information from both real and reciprocal spaces, spectroscopy can be locally carried out (microspectroscopy), or the spectroscopic information can be used to create contrast in real-space images (spectromicroscopy). Alternatively, when the sample is illuminated with the electron beam, the energy filter can be used to perform spatially resolved electron energy loss spectroscopy experiments.

First experimental results

Initial experiments performed with ESCHER during the installation phase concerned the growth of graphene on a 4H-SiC(0001) substrate (see, e.g., [7]). Graphene was formed *in situ* by heating the SiC substrate to about 1,700 K [7]. Bringing the sample to these elevated temperatures causes the desorption of Si from the sample surface. The carbon atoms left behind on the surface rearrange to form a thin graphene film with a thickness in the range of 1–4 atomic layers. **Figure 2(a)** shows step edges of the SiC substrate at an electron energy at the sample of $E_0 = 2.5$ eV.

Figure 2(b) shows an image of the same area of the sample at a slightly higher electron energy of $E_0 = 4.5$ eV. We note the remarkable change in contrast. From the literature, we know that the change of contrast as a function of electron energy allows one to determine the number of monolayers of graphene at each position on the sample [8]. Such an analysis reveals that the bright and dark areas in Figure 2(b) correspond to one monolayer and two monolayers of graphene, respectively. Both images show a field of view of about $4.5 \mu\text{m}$. For these images, the spatial resolution is limited not by the electron optics but by the spatial resolution of the multichannel plate (MCP) electron detector.

Resolution

In this section, we discuss the ultimate resolution for aberration-corrected LEEM in theory and in a real experiment. Recently, a wave-optical approach for image calculations in aberration-corrected electron microscopes has been introduced [9]. This approach is based on the contrast transfer function (CTF) formalism, which has been in use in the transmission electron microscopy community for more than 30 years, for the case of weak-phase objects. Here, the image modifications introduced by the system are considered by the CTF in an analytical form. The two main causes for these modifications are, on the one hand, spherical and chromatic aberrations of the objective lens and,

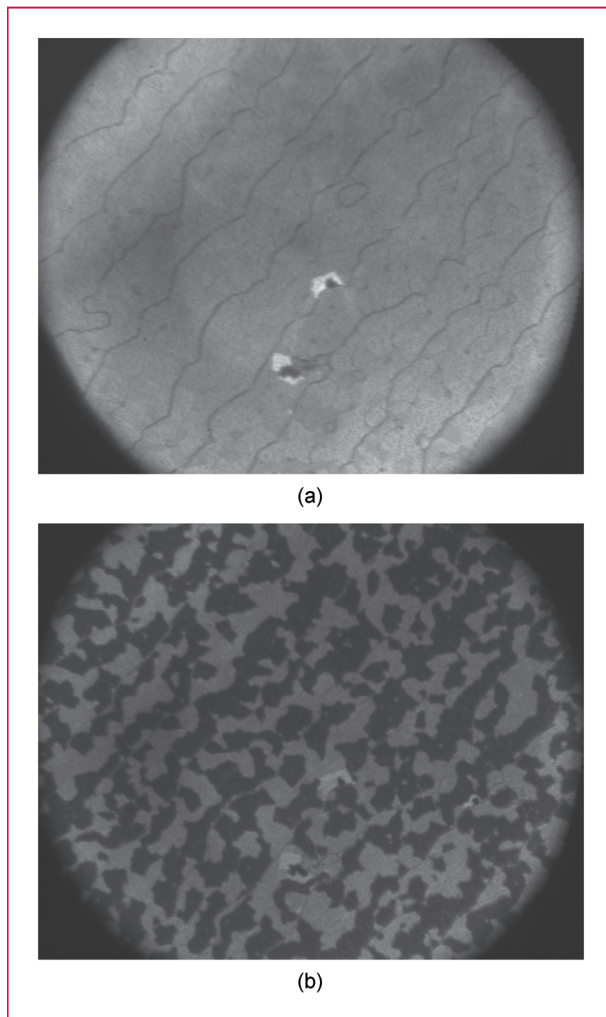


Figure 2

LEEM images of the same area of a SiC(0001) sample covered with a few monolayers of graphene taken with the ESCHER setup: (a) Step edges at the substrate are visible. The electron energy is $E_0 = 2.5$ eV. (b) The bright areas correspond to one monolayer, and the dark areas to two monolayers of graphene. The electron energy is $E_0 = 4.5$ eV. The field of view is approximately $4.5 \mu\text{m}$.

on the other hand, the cutoff of high-spatial-frequency components by the contrast aperture in the diffraction plane. The image intensity I of a given object $f(r)$ is given by $I = |f(r) \otimes h(r)|^2$, where \otimes indicates the convolution between $f(r)$ and $h(r)$, the latter representing the inverse Fourier transform of the CTF of our microscope [9].

Figure 3(a) shows the calculated resolution of a $1:1/\sqrt{3}$ amplitude object as a function of aperture angle for non-aberration-corrected (black line) and aberration-corrected (red line) LEEM. A $1:1/\sqrt{3}$ amplitude object is an object where the image amplitude is 1 for $x < 0$ and $1/\sqrt{3}$ for $x \geq 0$, leading to an image intensity ratio

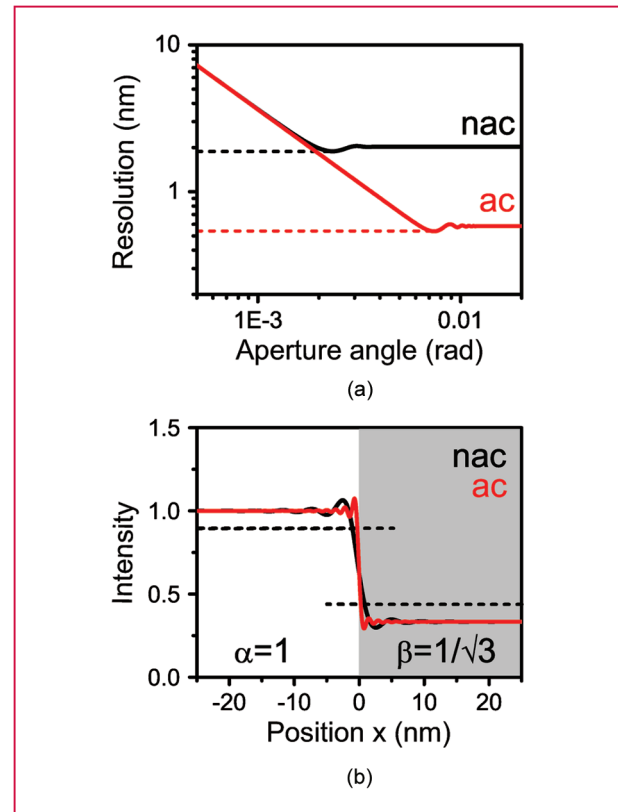


Figure 3

(a) Resolution and (b) image intensity profiles for an object with an object amplitude $\alpha = 1$ for $x < 0$ and an object amplitude $\beta = 1/\sqrt{3}$ for $x \geq 0$. The electron energy spread is $\Delta E_0 = 0.25$ eV, the electron energy at the sample is $E_0 = 10$ eV, and the calculations are performed for zero defocus. (a) LEEM resolution as a function of aperture angle for (black line) non-aberration-corrected (nac) and (red line) aberration-corrected (ac) optics. (b) Image intensity profiles with aperture angles of 2.34 and 7.37 mrad for (black line) non-aberration-corrected (nac) and (red line) aberration-corrected (ac) LEEM, respectively. (Horizontal dashed lines) Intensity values corresponding to 84% and 16% of $|\alpha^2 - \beta^2|$, as used to obtain the spatial resolution plotted in (a). Aberration correction gives rise to improved spatial resolution and a much finer fringe spacing in the intensity profile.

(amplitude squared) of 3. Furthermore, the phase of the electrons leaving the sample is taken to be invariant with x . Here, we define the resolution of an $\alpha:\beta$ amplitude object at a given aperture angle as the lateral separation between 84% and 16% of the step size. Note that all calculations presented here are performed for an electron energy at the sample of $E_0 = 10$ eV and an energy spread of the electron source of $\Delta E_0 = 0.25$ eV—a typical value for cold-field emitters. We perform the calculation of the image intensity as a function of x for a series of different aperture angles α . The resolution was extracted from the corresponding 1-D images for each aperture angle. In addition to the electron

energy, the spherical and chromatic aberrations of the objective lens and the electron mirror up to the fifth order are entered into the calculation. The defocus of the objective lens was set to zero. Using these parameters, we obtain the plots in Figure 3(a) for non-aberration-corrected (nac; black line) and aberration-corrected LEEM (ac; red line). The graphs show the resolution as a function of aperture angle α . The resolution closely follows a $0.38\lambda/\alpha$ behavior for small aperture angles, due to the k -space cutoff by the contrast aperture (often called the diffraction limit). For larger aperture angles, the resolution starts to oscillate until it remains constant. This is caused by the damped oscillations of the CTF at larger k values, as explained in [9]. We find that the ultimate resolution, i.e., the global minima in Figure 3(a), is 1.9 and 0.5 nm for non-aberration-corrected and aberration-corrected LEEM, respectively. The image intensities with the ultimate resolution are shown in **Figure 3(b)** for non-aberration-corrected (black line) and aberration-corrected (red line) electron optics. These image profiles are calculated at the optimum aperture size of 2.34 and 7.37 mrad for non-aberration-corrected and aberration-corrected LEEM, respectively, at magnification $M = 1$. Intensity fringes around the amplitude step at $x = 0$ can be observed in these images. The amplitude of the intensity fringes decays with increasing distance from the step position. More intensity fringes with higher oscillation frequencies are observed for the aberration-corrected case, as compared with the non-aberration-corrected LEEM, as the larger contrast aperture transmits larger k -values, i.e., higher spatial frequencies.

So far, the best resolution obtained in an aberration-corrected LEEM experiment is approximately 2 nm [5]. Our goal is to reach this same resolution with ESCHER in routine operation in the near future. A longer term aim is to further improve the resolution to <1 nm, which is close to the theoretical limit. In order to reach this performance, several measures have to be taken to reduce the level of vibrations introduced into the system and to increase mechanical stability. First, we are developing a new sample stage. This new stage will be directly attached to the objective lens, eliminating any direct mechanical coupling to other parts of the vacuum system. In addition, we will incorporate a mu-metal shield around the sample to suppress electromagnetic disturbances. In the vicinity of the sample, shielding is most important since the electron energy is at its lowest value. Such magnetic shielding is absent in the present microscope. In addition, the vibration and the acoustic isolation of the microscope have to be optimized. The system is already installed on its own vibration-isolated building foundation and is equipped with an active vibration isolation system (AVI-400/LP and AVI-350/LP from TABLE STABLE, Switzerland). Vibrations transmitted through incoming wires, tubes, and vacuum pumps have yet to be minimized. Moreover, acoustic isolation becomes

increasingly important to reach the ultimate resolution. Other sources of interference include alternating-current magnetic fields that are present in the vicinity of the microscope. Even small fields can cause oscillatory displacements of the image and therefore degrade the resolution. This can be overcome by improving the passive magnetic shielding, particularly of the sensitive magnetic prism arrays. Furthermore, the stability of the power supplies of the microscope needs to be better than 0.1 ppm. Finally, the image detection system has to be improved to reach a resolution as low as 1 nm at a field of view of $1\ \mu\text{m}$, i.e., the detector must be able to resolve 1,000 pixel elements across the field of view. MCP/phosphor/charge-coupled device camera detector systems currently in use in most LEEM/PEEM instruments have a spatial resolution of about $130\ \mu\text{m}$ across a 40-mm diameter detector. This gives only 300 resolvable pixel elements across the detector. An attractive replacement of this commonly used detection system is the Medipix detector—a solid-state pixel detector. In the framework of the ESCHER project, it has already been shown that the detector resolution of Medipix is better by about a factor of 2, as compared with a standard MCP-based detector [10]. **Figure 4** shows LEEM images of graphene flakes grown on an Ir(111) substrate recorded with the LEEM setup at the University of Twente. The image in Figure 4(a) was recorded with a conventional MCP detection system, and the image in Figure 4(b) was recorded with a Medipix2 detector. Both images show the same sample area at identical electron-optical magnification. It is clear from these images that finer image details are visible in the image taken with Medipix2.

Cryogenic LEEM

LEEM has proven to be a very powerful technique to study dynamic processes at surfaces, such as phase transitions and growth phenomena *in situ* at elevated temperatures [1–4]. There are, however, also numerous interesting phenomena that take place at temperatures below room temperature. For example, complex oxides with their rich phase diagrams show magnetic and electronic phase transitions at low temperatures [11]. Nucleation and growth phenomena at low temperatures are also interesting topics due to strongly decreasing diffusion coefficients with decreasing thermal energy.

Present-day LEEM systems generally have a limited temperature range of the sample, extending from 300 K to about 1,800 K. Only a few LEEM/PEEM systems exist with the capability of cooling the sample below room temperature but typically not lower than 100 K. The lowest temperature achieved in a LEEM experiment, which was obtained with a liquid helium (LHe) cooled sample stage, is around 50 K [12]. One goal of the ESCHER project is to build a LEEM sample stage with the capability of maintaining the sample at a temperature in the entire range

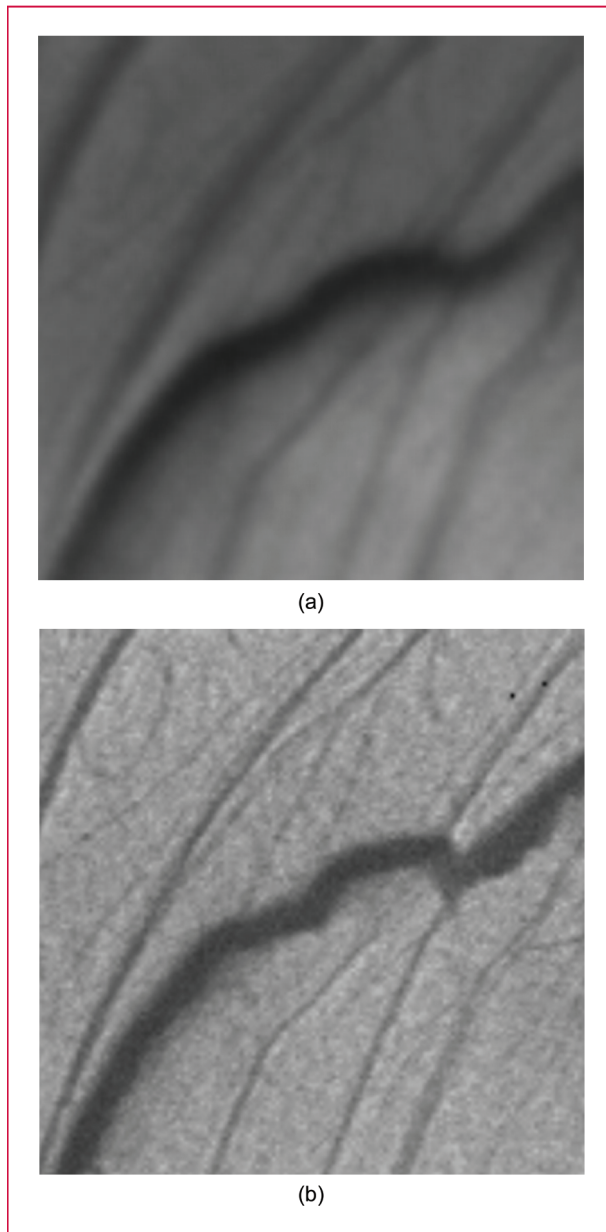


Figure 4

LEEM images of graphene flakes on Ir(111) recorded with (a) a conventional MCP detector and (b) a Medipix2 detector with the LEEM setup at the University of Twente. Both images show the same sample area at identical magnification with a field of view of $1.5 \mu\text{m}$. The detector resolution is improved by about a factor of 2 in the case of Medipix2.

between 10 and 300 K. This low-temperature stage will be located in the sample chamber on the left-hand side of the first prism array [see Figure 1(c)].

A major challenge that has to be met is that the mechanical alignment of the low-temperature sample stage has to be

precise and stable with respect to the gun/projector column, which remains at 300 K. Yet, it is desirable to minimize heat conduction through rigid mechanical mounts. In addition, positioning of the sample, biased with a high voltage of about -15 kV , is required with 5 degrees of freedom with respect to the objective lens. Furthermore, potential vibrations from the cooling mechanism have to be suppressed to a level that will not compromise the desired lateral resolution.

Figure 1(b) shows a schematic of our current design concept. Both the objective lens and the sample, including the stage, will be cooled. The objective lens and the sample stage are only cooled with liquid nitrogen (LN_2), whereas the sample and its immediate vicinity will be cooled with LHe. To minimize dissipation of heat in the objective lens, the copper coil that excites the electromagnetic objective lens will be replaced with a superconducting coil with a high critical temperature. With the objective lens at LN_2 temperature, radiative heat transfer from the objective lens to the sample and the sample stage will be minimized. This will reduce the sample drift as much as possible, and the stability of the sample temperature will be improved. Furthermore, cryogenic pumping by the sample will be reduced, and the base temperature at the sample will be lower. An LN_2 -cooled envelope of the sample environment will minimize consumption of precious LHe resources. This cryogenic shield also acts as a passive magnetic shield around the sample space. The sample holder itself will have a miniature integral heater element that will enable temperature control between 10 and 300 K. For experiments between room temperature and 77 K, the sample can be cooled with LN_2 only.

Upon successful completion of the cryogenic sample stage, the ESCHER setup will give access to physical phenomena at a very broad temperature range from 10 to 1,800 K. This allows one to perform a vast number of novel and interesting experiments. We expect the low-temperature setup to be operational by year-end 2011.

Summary

We have described the layout and the capabilities of a new aberration-corrected LEEM and spectroscopy facility, i.e., ESCHER, at Leiden University. Initial experimental results obtained on thin graphene films grown *in situ* on SiC(0001) at 1,700 K are very promising and demonstrate that the electron optical system is fully operational. In our quest for the ultimate spatial resolution, we have shown image and resolution calculations with a wave-optical formalism, taking into account aberrations up to the fifth order. From this, we have concluded that the theoretical resolution limit in aberration-corrected LEEM is around 0.5 nm. This is better than the experimental record by a factor of 4. We have addressed the various factors that limit the experimental resolution and have discussed what measures we will take

to improve it toward the theoretical limit. Finally, we have introduced a schematic design concept for the cryogenic LEEM environment that is currently under development. It will have the possibility of controlling the sample temperature in the range from 10 to 300 K. This will give us access to physical phenomena over an exceptionally broad temperature range between 10 and 1,800 K.

Acknowledgments

The authors would like to thank R. van Egmond (Fine Mechanical Department, Leiden University), M. Hesselberth, and D. Boltje (both from Leiden University) for their help and support during the installation and startup of the LEEM system; J. Visser (Nikhef), R. van Gastel and B. Poelsema (Twente University), and J. I. Sikharulidze and P. Abrahams (Leiden University) for their collaboration in the Medipix project; and J. M. van Ruitenbeek (Leiden University) for insightful discussions. This work was supported by the Netherlands Organization for Scientific Research (NWO) under an NWO-Groot Grant and a Vidi Grant (Sense Jan van der Molen).

References

1. E. Bauer, "Low energy electron microscopy," *Rep. Prog. Phys.*, vol. 57, no. 9, pp. 895–938, Sep. 1994.
2. R. M. Tromp, "Low-energy electron microscopy," *IBM J. Res. & Dev.*, vol. 44, no. 4, pp. 503–516, Jul. 2000.
3. R. J. Phaneuf and A. K. Schmid, "Low-energy electron microscopy: Imaging surface dynamics," *Phys. Today*, vol. 56, no. 3, pp. 50–55, 2003.
4. J. B. Hannon and R. M. Tromp, "Low-energy electron microscopy of surface phase transitions," *Annu. Rev. Mater. Res.*, vol. 33, pp. 263–288, 2003.
5. R. M. Tromp, J. B. Hannon, A. W. Ellis, W. Wan, A. Berghaus, and O. Schaff, "A new aberration-corrected, energy-filtered LEEM/PEEM instrument. I. Principles and design," *Ultramicroscopy*, vol. 110, no. 7, pp. 852–861, Jun. 2010.
6. R. M. Tromp, Y. Fujikawa, J. B. Hannon, A. W. Ellis, A. Berghaus, and O. Schaff, "A simple energy filter for low energy electron microscopy/photoelectron emission microscopy instruments," *J. Phys.: Condens. Matter*, vol. 21, no. 31, p. 314007, Aug. 2009.
7. R. M. Tromp and J. B. Hannon, "Thermodynamics and kinetics of graphene growth on SiC(0001)," *Phys. Rev. Lett.*, vol. 102, no. 10, p. 106 104, Mar. 2009.
8. H. Hibino, H. Kageshima, F. Maeda, M. Nagase, Y. Kobayashi, Y. Kobayashi, and H. Yamaguchi, "Thickness determination of graphene layers formed on SiC using low-energy electron microscopy," *e-J. Surf. Sci. Nanotech.*, vol. 6, pp. 107–110, 2008.
9. S. M. Schramm, A. B. Pang, M. S. Altman, and R. M. Tromp, "A contrast transfer function approach for image calculations in aberration-corrected LEEM and PEEM," *Ultramicroscopy*, 2011, submitted for publication.
10. R. van Gastel, I. Sikharulidze, S. Schramm, J. P. Abrahams, B. Poelsema, R. M. Tromp, and S. J. van der Molen, "Medipix 2 detector applied to low energy electron microscopy," *Ultramicroscopy*, vol. 110, no. 1, pp. 33–35, Dec. 2009.
11. B. G. Levi, "Interface between nonmagnetic insulators may be ferromagnetic and conducting," *Phys. Today*, vol. 60, no. 6, pp. 23–27, 2007.
12. M. S. Altman, *Low Energy Electron Microscopy*. [Online]. Available: <http://physics.ust.hk/department/phaltman/leem/>

Received October 15, 2010; accepted for publication February 1, 2011

Sebastian M. Schramm *Leiden University, Kamerlingh Onnes Laboratorium, NL-2300 RA Leiden, The Netherlands (schramm@physics.leidenuniv.nl).*

Jaap Kautz *Leiden University, Kamerlingh Onnes Laboratorium, NL-2300 RA Leiden, The Netherlands (kautz@physics.leidenuniv.nl).*

Andreas Berghaus *SPECS GmbH, Voltastrasse 5, D-13355 Berlin, Germany.*

Oliver Schaff *SPECS GmbH, Voltastrasse 5, D-13355 Berlin, Germany (Oliver.Schaff@specs.com).*

Rudolf M. Tromp *Leiden University, Kamerlingh Onnes Laboratorium, NL-2300 RA Leiden, The Netherlands; IBM Research Division, Thomas J. Watson Research Center, Yorktown Heights, NY 10598 USA (rtromp@us.ibm.com).*

Sense Jan van der Molen *Leiden University, Kamerlingh Onnes Laboratorium, NL-2300 RA Leiden, The Netherlands (molen@physics.leidenuniv.nl).*